Chapter 16
Effect of Porosity on Ion Transport Through Polymers and Polymer-Based Composites Containing Inorganic Nanoparticles (Review)

Yuliya Dzyazko, Yurii Volfkovich, Olga Perlova, Ludmila Ponomaryova, Nataliia Perlova, and Evgen Kolomiets

16.1   Introduction

The development of nanotechnologies gives a new impulse to chemistry of polymer ion exchange resins and membranes, which are related to nanomaterials. When they are in contact with water or other polar solvent, the system of nanopores is formed. First, this feature has been found for homogeneous perfluorinated membranes (PFMs) of Nafion type [1, 2]. Then, it was proved for other polymer ion exchange materials (heterogeneous membranes and resins) [3, 4]. The nanopores are hydrophilic; they provide ion transport and ion exchange ability of swollen polymers. Their porous structure involves also hydrophobic pores; their size is from several tens of nanometers to several tens of microns. Both hydrophilic and hydrophobic pores are available for any inorganic modifier: the filler affects functional properties of the composite. The most intensive work in the field of practical application of organic-inorganic ion exchange materials has been started since the 2000s [5]. The necessity of investigations was caused by requirements of technologies for alternative energy and separation.

Y. Dzyazko · E. Kolomiets
VI Vernadskii Institute of General and Inorganic Chemistry of the National Academy of Science of Ukraine, Kyiv, Ukraine

Y. Volfkovich
AN Frumkin Institute of Physical Chemistry and Electrochemistry of the RAS, Moscow, Russia

O. Perlova · N. Perlova (✉)
Odessa II Mechnikov National University, Odesa, Ukraine

L. Ponomaryova
Sumy National University, Sumy, Ukraine

Correctly chosen ion exchange support, inorganic modifier, and modification technique allow one to accelerate ion transport through the polymer materials, expand the range of operation temperature, increase ion exchange capacity, and enhance selectivity of the composites [6]. Since porous structure of polymer ion-exchanger and membranes is very complex, inorganic particles can be in one or other pores. Thus, their effect on the porous structure and functional properties of polymer support can be different. This problem is outside the focus of attention except probably [7].

16.2   Dry and Swollen Ion Exchange Polymers: Swelling Pressure

Dry ion exchange materials contain heterogeneities that are formed during synthesis [1, 2, 8, 9]. Dipole-dipole interaction between fixed ions and counter-ions results in multiplet (cluster) formation. Different estimations give 2–8 pairs in the multiplets [8, 9].

The nanosized heterogeneities in dry polymers were recognized by small-angle X-ray scattering (SAXS) [2, 10], and the method of small-angle neutron scattering was also applied [11]. The spectra show two peaks at scattering vector of 0.01–0.1 A^{-1} indicating a size of the formations of several nanometers and several tens of nanometers. The smallest heterogeneities are related to clusters, and the larger ones are associated with crystallinity (the larger the crystallinity, the more distinct is the SACS maximum) [10]. The last formations and also claw-like structure defects can be observed using scanning electron microscopy (SEM) [12] as seen in Fig. 16.1a. In the case of macroporous resins, structure defects of micron size are formed purposefully in ion exchange polymer during synthesis.
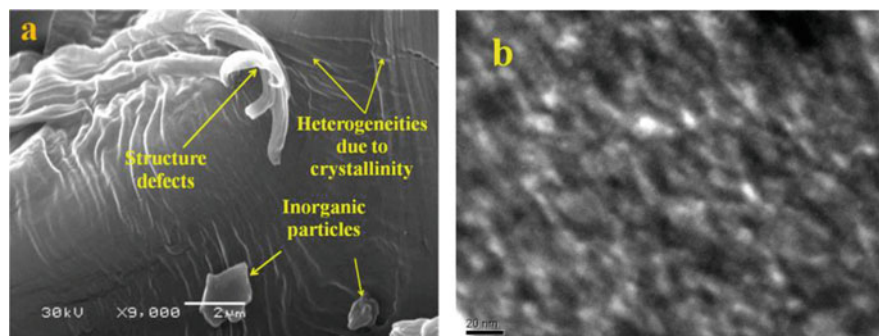

Fig. 16.1 SEM (**a**) and TEM (**b**) images of CMI-7000 cation exchange membrane (**a**, adapted from [13]) and Dowex HCR-S gel-like cation-exchange resin (**b**, original photo)

There are pores, the size of which is several tens of microns, in heterogeneous membranes [5, 13, 14]. They are attributed to voids between ion-exchanger and binder. The macropores of dry polymers are recognized with mercury porosimetry [15]. The smallest heterogeneities are visualized with transmission electron microscopy (TEM) (Fig. 16.1b) after shading with transition metal ions [12].

Thus, the structure of dry ion exchange polymers contains practically no micro- and mesopores, however, macropores are characteristic for them.

Thermodynamic approaches to swelling of ion exchange materials were summarized by Helfferich in 1950s [16]. A solution of water in polymer has been suggested. In other words, water and polymer are not different phases; no nanopores are related to swollen ion-exchanger.

According to modern approaches, swelling of ion exchange polymers is multistage. Primarily, functional groups (for instance, $-SO_3H$) are hydrated forming the pairs of fixed ions ($-SO_3^-$) and H_3O^+ counter-ions [17]. Next water molecules join H_3O^+ forming clusters of counter-ions with several H_2O molecules. Continuous aqueous phase is formed by this manner. Water and polymer are different phases, as proved by Hsu and Gierke based on SAXS data for Nafion PFM [2]. The model of nanopores (alternating nanosized clusters, which are formed from the smallest heterogeneities of dry polymers, and smaller channels) has been proposed (Fig. 16.2). The clusters and channels are organized similarly to inverted micelles (ion exchange groups are inside them) and arranged on a lattice. In other words, hydrophilic fragments of hydrocarbonic chains form the so-called gel regions, which are penetrated by clusters and channels. The nanopores are responsible for ion transport – they are called "transport pores."
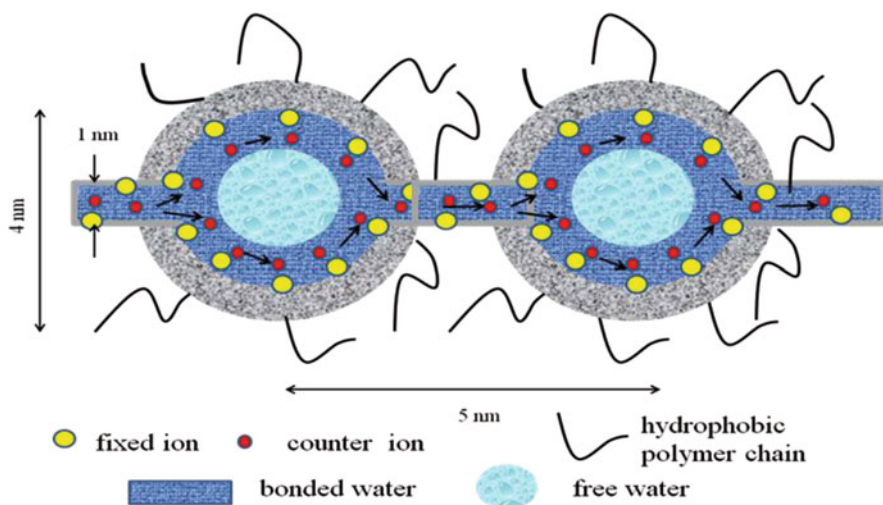

Fig. 16.2 Cluster-channel model for ion exchange polymer. Arrows show ion transport through Debye's layer along pore walls

Despite some criticism and alternative approaches [18], the Hsu-Gierke model has endured for many years as a conceptual basis for rationalizing the properties of Nafion-type, membranes, especially ion and water transport. The approach was developed further. Parallelism of cluster-channel paths [19] as well as aggregation and agglomeration of clusters [10] were suggested. The Hsu-Gierke model was also applied not only to homogeneous PFMs, but also to ion exchange resins and heterogeneous membranes [3, 4, 20].

Transport pores contain bonded water, namely, water clusters around fixed and counter-ions. A thickness of its layer is 1.5 nm [20]. Ion movement along pore walls is slower comparing with aqueous solutions. The cluster centers are filled with free water, in which the transport rate is close to that for aqueous solutions.

According to [21], the ion transport occurs through clusters and channels, where the distribution of counter- and co-ions is irregular. Regarding a cation-exchanger, this is caused by negative charge of pore walls due to fixed ions on them. The negative charge is compensated by adjacently located positively charged counter-ions. The thickness of this Debye's layer is about 1 nm. Anions and nonpolar molecules are excluded from it. When the ion-exchanger is in contact with a concentrated solution, there is almost electrically neutral liquid in the pore center (cations and anions are in equal amounts). The conductivity of the ion exchanger materials is predominantly determined by transport of counter-ions through the Debye's layer along pore walls (see Fig. 16.2), but co-ions and nonpolar molecules moved through free solution in the centers of pores.

As opposed to Ref. [21], the Debye's layers in clusters are overlapped, when an outer solution is low-concentrated. Ions move not only along pore walls but also through free water in the centers. In this case, the ratio of clusters and channels plays a key role due to different mobility of counter-ions in free and bonded water [12, 14, 22, 23]. However, the approach [21] is important for electrodialysis, when at least one side of a membrane is in contact with rather concentrated solution.

Porous structure of swollen ion exchangers involves also voids between gel regions, which are formed by bundles of hydrophobic fragments of polymer chains. Other elements of porosity are macropores, which are also attributed to dry polymers. Both gel regions and macropores are filled with a neutral solution. Ions of this solution make insignificant contribution to transport [12, 20, 22, 23]. This causes selectivity of ion exchange membranes toward either cations or anions [20]. As shown theoretically, the transport number of charged species is equal to the contribution of clusters and channels to total porosity [24]. Pores, a radius (r) of which is less than 10 nm, determine charge selectivity of membranes. The approach has been confirmed experimentally [7].

In fact, fixed and counter-ions in hydrophilic pores are osmotic centers. The osmotic theory of swelling suggests concentrated electrolyte inside transport pores, when the ion-exchanger is in contact even with pure water [16]. The "solution" is able to be diluted. In this case, the Debay's layers are overlapped in the clusters; thus the transport pores are filled with a "solution."

In the framework of macroscopic models, the tendency of the "solution" to be diluted is considered as the difference between the osmotic pressures of the

liquids inside and outside the granules of resin or the membrane sheets (so-called swelling pressure, π according to Gluekauf and Gregor models). The π value has been suggested for the ion-exchange materials, which change their volume freely. This magnitude has not to be related to the swelling pressure of gel in a volume bounded with rigid walls, as valid for polymers [25]. When water content in the ion-exchanger increases, osmotic pressure decreases [16]:

$$\pi v_{H_2O} = -RT \ln a_{H_2O}, \tag{16.1}$$

where a_{H_2O} is the activity of water in the ion-exchanger (related to free water, $a_{H_2O} = 1$ outside granules, $a_{H_2O} < 1$ inside them [26]), R is the gas constant, T is the temperature, and v_{H_2O} is the partial molar volume of water.

Elastic pressure, which is attributed to the polymer net, grows with increase of water content. This magnitude is estimated quantitatively according to Flory-Rehner theory [27]. When the values of osmotic and elasticity pressure become equal, the swelling stops.

The π value for any ion-exchanger can be calculated, when this magnitude is known for other sample of similar composition, and the water content in two samples is equal. The swelling pressure grows linearly with increase of cross-linkage [16]. Regarding strongly acidic gel-like cation-exchangers produced by Dow Chemical Company, this magnitude is $\approx$50 bar for the resin containing 4% of divinylbenzene, 150 bar (8%), 350 bar (16%), and 650 bar (24%). The Nafion PFM shows higher swelling pressure than the resin containing 8% of DVB [28].

16.3   Purposeful Formation of Inorganic Particles in Ion Exchangers

Depending on interaction of inorganic constituent with polymer, the organic-inorganic materials are divided into two classes [29, 30]. In class I, the components are bonded together through strong covalent or coordinative bonds: the inorganic fragments can be built-in a polymer backbone or grafted to it. Alternately, the inorganic matrix can be functionalized with organics. Regarding class II, inorganic and polymer constituents are different phases. The interactions between them are hydrogen bonding, van der Waals, π–π or weak electrostatic attraction. The materials of class II are related to composites. They can be obtained by solution-casting using finely dispersed inorganic ion-exchanger and sol-gel technique that often provides simultaneous formation of both polymer and inorganic constituents. Inorganic particles can be also embedded to the preliminarily synthesized polymer. In the last case, it is possible to use any commercial ion exchange material. Any inorganic constituent can be inserted into the polymer, if the synthesis method provides no its destruction. Since complex porous structure is attributed to ion exchange polymers, the particles can be deposited in one or other types of pores.

The features of precipitation of zirconium hydrophosphate (ZHP) and hydrated zirconium dioxide (HZD) are analyzed in Refs. [31, 32]. As an example, let us consider ZHP deposition: the synthesis method involves impregnation of polymer with a $ZrOCl_2$ solution followed by treatment with phosphoric acid. For simplicity, denote ZHP as $CatAn_z$ (where z is the charge number) and assume that there are only $H_2PO_4^-$ ions in the precipitator solution (HAn).

During precipitation, dissolution of small particles and their reprecipitation on larger particles is advantageous from a thermodynamic point of view. Gibbs energy of the system reduces due to decrease of the particle surface. The Ostwald-Freundlich Eq. [33] reflects the effect of the radius of particles (r_p) on their solubility:

$$\ln \frac{\overline{C}_{CatAn_z}}{C_{CatAn_z,\infty}} = -\frac{\beta V_m \sigma \cos \varphi}{RT r_p} \tag{16.2}$$

Here $\overline{C}_{CatAn_z}$ and $C_{CatAn_z,\infty}$ are the concentration of dissolved compound in the ion-exchanger and its saturated solution, respectively; β is the shape factor of particles, V_m is the molar volume of $CatAn_z$, σ is the surface tension of solvent, and φ is the wetting angle (≈ 1 for hydrophilic compound).

The equations that take into consideration the conditions of precipitation have been proposed [31, 32]. They include the concentration of metal salt (C_{Cat}) and precipitator (C_{pr}), the volumes of ion-exchanger (V_i) and precipitator (V_{pr}), the solubility product of $CatAn_z$ (K_{sp}), and the exchange capacity of polymer [31]:

$$r_p = -\frac{\beta V_m \sigma \cos \varphi}{RT \left[\ln K_{sp} - \ln C_{CatAn_z,\infty} - z \ln \left(C_{pr} - \frac{(A+zC_{Cat})V_i}{V_{pr}} \right) \right]} \tag{16.3}$$

As follows, smaller particles are formed in the ion-exchanger with higher exchange capacity. For instance, the composite based on rigid resin contains smaller ZHP particles than flexible polymer (Fig. 16.3). However, Eq. (16.3) shows only the way that allows us to control the particle size; the formula gives no possibility for exact calculations. This is mainly due to ambiguity of the K_{sp} value for multivalent metal ions. For example, a large variety of species were found in the solution over HZD precipitate: $Zr(OH)_3^+$, $Zr(OH)_2^+$, $Zr(OH)_3^+$, $Zr(OH)_4(aq)$ as well as the polymeric species $[Zr_4(OH)_8]^{8+}$ and $Zr_2(OH)_2^{6+}$ [34]. Different dissolution reactions, which is characterized by own K_{sp}, have to be considered.

However, we can estimate the particle radius for HZD from Eq. (16.2). The ratio under logarithm (the content of Zr in the solution for undersaturation and oversaturation conditions) is not higher than 0.1 [35]. We can assume $V_m = 21.6$ cm^3 mol^{-1} for amorphous HZD similarly to crystalline ZrO_2. Since $\beta = 2.8$ for globules, the minimal particle diameter is 1.6 nm for the temperature of 293 K.

When sol of insoluble neutral zirconium hydroxocomplexes is used for impregnation of ion-exchanger (oversaturation condition), the ratio at the left side of Eq. (16.2) is close to 1, and the logarithm is close to 0. Since $z = 0$, Eq. (16.3)
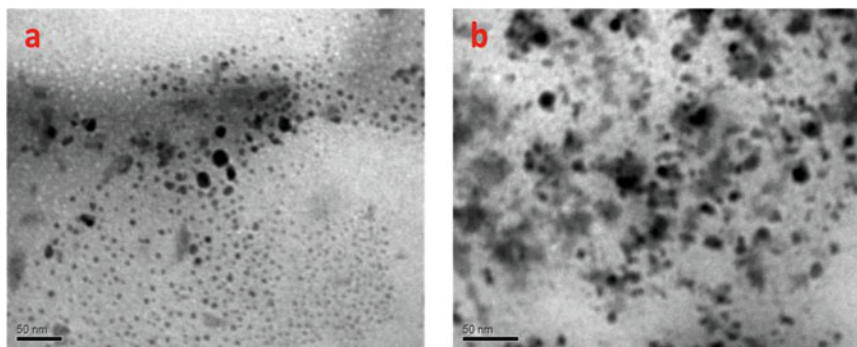
Fig. 16.3 TEM images of ZHP nanoparticles in rigid (Dowex HCR-S) and flexible (Dow WX-2) resins. (Adapted from Ref. [31])

is simplified down to Eq. (16.1). As a result, large particles of micron size are deposited inside ion-exchangers [23]. No single nanoparticles were found, though sol contained very small single particles ($\approx$6 nm) [36]. Comparing with ZrO_2, α-ZHP is characterized by larger molar volume (91 cm^3 mol^{-1}) as calculated in Ref. [37]. The sufficient difference in molar volume is probably attributed for amorphous ZHP and HZD. Larger ZHP particles are formed in the substrate of microfiltration membrane [37, 38]. Smaller HZD particles are precipitated also in active layer improving rejection ability of the membrane.

The formation of the amorphous modification of ZHP and titanium hydrophosphate (THP) in polymers is suggested [39, 40]. Under certain synthesis conditions, crystalline modifications can be formed [41–43]. ZHP crystallizes in hydrophobic pores of Nafion PFM, amorphous modification is formed in clusters and channels [43]. Both hydro- and dihydrophosphate groups (attributed to α- and γ-ZHP modifications, respectively) were found with NMR spectroscopy: the spectra show two signals [23, 44] similarly to individual amorphous ZHP [45]. More complex spectra were obtained for PFM containing single nanoparticles [44]. The signals at -15 and -20 ppm are suggested to be related to crystalline ZHP; other signals correspond to amorphous phase.

As shown further, the state of embedded particles (non-aggregated nanoparticles, aggregates or agglomerates) affects porosity of the polymer on the one hand and ion transport through the composite on the other hand.

16.4   Investigations of Porous Structure of Polymer-Based Composites

Since main pores of polymers ion-exchangers are formed only in a solvent, special techniques are necessary. Regarding membranes, Archimedes' (picnometer) method [46] is enough to determine total porosity including closed pores.

Fractions of transport (α) and non-transport pores can be determined from the measurements of electrical conductivity ($\overline{\kappa}$) using heterogeneous model [20], which involves the conductivity of gel regions (κ_g) and equilibrium solution (κ):

$$\overline{\kappa} = \kappa_g^{\alpha} \kappa^{1-\alpha}. \tag{16.4}$$

Mercury is used as non-polarized electrodes; resistance at the membrane-solution interface is excluded by this manner. The conductivity of gel regions is calculated for Isoconductivity point, where $\overline{\kappa} = \kappa$. Linearity of $\log \overline{\kappa}$-$\log \kappa$ curve means that the $\overline{\kappa}$ and κ values are close to each other, and the model is valid. The conductivity of gel regions and the α-parameter are determined from the logarithmic dependence.

Exclusion of the effect of the membrane-solution interface is especially important to estimate transport and non-transport pores. The model cannot be applied without complying with this condition [13, 14]. In this case, the curve is modeled using semilogarithmic dependence.

Detailed analysis of pore size distributions (up to $r = 100$ nm) is possible by means of the method involving water adsorption-desorption using a vacuum Mac-Ben apparatus supplied with quartz scales [47]. Isotherms are obtained by this manner [16]. Further they are recalculated into integral and differential pore size distributions using the algorithm [47].

Other techniques are isopiestic method [48] and thermoporosimetry based on differential scanning calorimetry (DSC) [49]. The last method, which gives information about pores, a radius of which is up to 3 μm, is described also in Ref. [15].

The method of standard contact porosimetry (MSCP), which has been recommended by the IUPAC [50], gives pore size distributions in a very wide interval ($r = 1$ nm–100 μm). The MSCP provides gravimetric measurements of the content of working liquid (water for polymers) in the sample. The measurements are performed also for the porous standards samples that are attached to the tested sample. The data corresponding to conditions of capillary equilibrium are taken into consideration. The amount of liquid in the system of standards and tested sample is varied by impregnation and drying. When thermodynamic equilibrium is reached, the liquid in the contacting porous materials has the same chemical potential. The pore size distributions for the tested sample can be recalculated from the known distribution for the standards. Theoretical approaches, which dealt the MSCP, and also some practical details are given in Refs. [15, 51–53]. Regarding the composite, all the abovementioned methods allow us to determine only porosity of polymer, since it destroys under the conditions of thermal pretreatment, which are necessary for dehydration of inorganic constituent.

16.5   Evolution of Porosity of Polymer-Based Composites

In order to investigate evolution of porous structure and functional properties of composites, stepwise modification of ion exchange resins with ZHP was performed [22, 23, 41, 54–56]. The water content in one or other types of pores of the polymer was determined by the MSCP. Figure 16.4a shows typical pore size distributions for individual ZHP and for the composites containing non-aggregated nanoparticles [56]. The curve for the inorganic ion exchanger demonstrates diffuse maximum at log $r \approx 0.3$ (nm). Regarding the composite, the area of the peaks for clusters and voids between gel regions decreases with the growth of ZHP content. No change of the peak centers is observed. Unchangeable position of these peaks is characteristic also for cation exchange membranes modified with silica [57] or ZHP [7]. This is a contradiction with a hypothesis by Yaroslavtsev and co-authors [58]. The surface of non-aggregated nanoparticles is covered with water, and additional water provides increase of size of clusters and channels. However, this hypothesis was not confirmed experimentally in Ref. [58] and subsequent works of these authors. Nevertheless Nagarale et al. [59] have found the increase of channel radius from 4 to 6 Å for polyvinyl alcohol (PVA) membrane, when the content of silica grows from 50% to 70%. The indirect method involving electroosmotic measurements followed by calculations via the formula:

$$r = \left(\frac{8\eta F \beta}{f_{cw}} \right)^{0.5} \tag{16.5}$$

where β implies that each coulomb of electricity exerts a drag effect, which is enough to carry β cm^3 of water through 1 cm^2 of the membrane, η is the viscosity coefficient for permeate, and f_{cw} is the coefficient of friction between counter-ion and water in a solution, $f_{cw} = RT/D$, where D is the diffusion coefficient of counter-ions in a solution. Thus, the hypothesis [58] is confirmed only for channels.
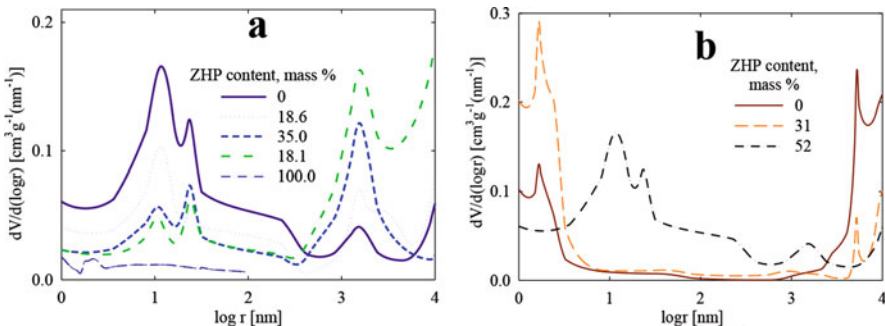

Fig. 16.4 Evolution of porous structure of Dowex HCR-S resin affected by ZHP. The composite contained non-aggregated nanoparticles. (**a**, Adapted from Ref. [56]), only aggregates and agglomerates (**b**, Adapted from Ref. [23])

As opposed to Refs. [22, 23], the increase of water content in transport pores and voids between gel regions has been found for the cation exchange membrane containing ZHP [7]. However, no information about the state of the embedded particles is given. Unreal low porosity (1.85×10^{-4} – 2.16×10^{-3}) has been reported for the membrane based on poly-*o*-toluidine containing Th(IV) phosphate [60].

When the composite contains only aggregates and agglomerates, the peaks due to mesopores are shifted toward lower log*r* values (Fig. 16.4b) [23]. The maximum of voids between gel fields is a shoulder of the cluster peak. The structure defects become larger comparing with the pristine resin, their volume increases after the first modification cycle. Further insertion of ZHP results in reduction of volume of macropores due to their filling with ZHP. The shift of the peaks attributed to mesopores is caused by swelling pressure in macropores due to additional osmotic centers (fixed and co-ions of the modifier). The constant position of cluster peaks for the composites containing also nanoparticles (see Fig. 16.4a) is due to additional swelling pressure in transport pores. This prevents their squeezing from the side of macropores.

As opposed to Refs. [22, 23], no influence of the modifier nanoparticles, which are located in transport pores, on structure defects has been found (the macropores were free from ZHP) [14]. The same effect is suggested in Ref. [7]; however, no information about the modifier state is given.

Comparing with MSCP, the method of water vapor adsorption gives lower pore volume and smaller clusters [61]. No shift of the cluster peaks is observed for the composite containing only large particles, since condensation of the vapor occurs only in micro- and mesopores providing lower swelling pressure (see Eq. (16.1)). The π value was estimated as 150 bar (pristine resin), 140 bar (resin filled with aggregates and agglomerates), and 190 bar (resin containing also single nanoparticles). Formally, non-aggregated nanoparticles can be considered as an additional cross-linking agent. The aggregates and agglomerates in hydrophobic pores "loosen" the resin structure. Similar results were obtained also with MSCP for rigid resin modified with large particles [55] and for flexible resin containing also non-aggregated nanoparticles [54].

16.6 Effect of Polymer Porosity on Ion Transport Through Composites

In order to establish the effect of incorporated inorganic particles on ion transport, some structure parameters of the polymer constituent have to be determined. One of them is the distance between functional groups (L) [24], which is determined taking into consideration the polymer fraction (m) in a composite, the exchange capacity of polymer (A_p) and its specific surface area (S):

Table 16.1 Parameters of porous structure for polymer and organic-inorganic ion exchange materials

Sample	Modifier, m	Particles[a]	L. nm	n[b]	α	γ	References
Ion exchange resin							
Dowex HCR-S	0	–	0.78	2.5	1.71	1.01	[22, 56, 61]
	ZHP, 0.39	NP, AR, AL	0.53	4.5	1.06	1.53	
	ZHP, 0.43	AR, AL	–	2.3	0.92	–	[23, 60]
Dowex WX-2	0	–	–	30.0	–	–	[54]
	ZHP, 0.21	NP, AR, AL	–	6.0	–	–	
Dowex MAC-3	0	–	0.37	4.3	0.4	0.6	[62]
	ZHP, 0.08	NP, AR, AL	0.38	3.9	0.4	0.9	
Membranes							
MK-40	0	–	–	5.8	1.9	1.6	[14]
	ZHP, 0.04	NP, AR		5.7	1.8	1.5	
MA-40	0	–		2.7	1.3	1.0	
	ZHD, 0.03	NP, AR		2.6	1.1	0.9	

[a]*NP* non-aggregated nanoparticles, *AR* aggregates, *AL* agglomerates
[b]The data were obtained with a method of water vapor adsorption (CC). Other results were obtained using MSCP

$$L = \left(\frac{qS}{A_p F (1 - m)} \right)^{0.5}, \qquad (16.6)$$

where q is the electron charge. The L parameter was applied to polymer membranes ($L = 0.4$–0.7 nm) [3, 7, 15, 20], membranes modified with HZD [14], and ion exchange resins and their composites [56, 62]. This and other parameters are summarized in Table 16.1. Figure 16.5a reflects the influence of this parameter on electric conductivity. The modified polymers demonstrate smaller L value than the pristine samples (see also Table 16.1). Modification with ZHP leads to increase [14] or even reduction of membrane conductivity [63], earlier no sufficient effect of the modifier has been found [64]. In the case of ion exchange resin, the influence of ZHP is unambiguous (Fig. 16.5b, see also Fig. 16.5a) [12, 22, 23].

Other parameter is a number of water molecules per functional groups (hydration number, n); it characterizes hydration of fixed and counter-ions [7, 15, 20, 57, 65]. For different membranes, $n = 3$–8 [65], 11 [57], 14–18 [7]. This value is calculated from the plateau of water adsorption isotherm [54, 55, 61]:

$$n = \frac{A_{H_2O}}{A_p V_{H_2O} (1 - m)}, \qquad (16.7)$$

where A_{H_2O} is the content of water. Modification of the membranes with silica causes significant increase of the n magnitude [57].
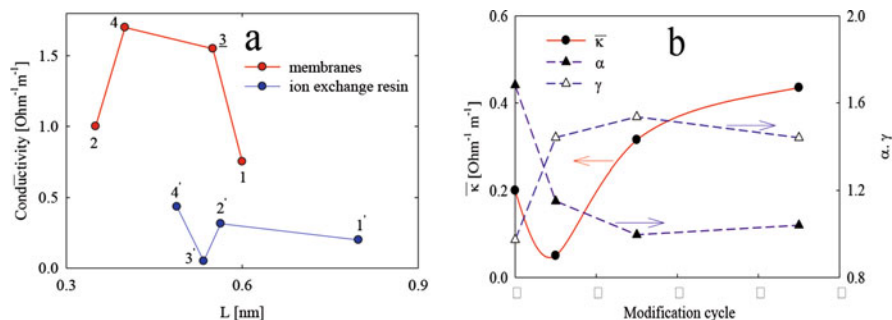
Fig. 16.5 Electrical conductivity of ion-exchange materials as a function of the distance between the functional groups of PFM (1–4, based on data [7]) and Dowex HCR-S resin ($1'-4'$, based on data [22, 56]) (**a**), conductivity, α- and γ-parameters vs modification cycle of Dowex HCR-S resin [22] (**b**). The modifier is ZHP; pouring (1, 2) and extruding (3, 4) membranes and pristine ($1, 1'$, 3) and composite ($2, 4, 2'-4'$) materials were researched, $m = 0.19(2'), 0.36(3'), 0.38(4')$
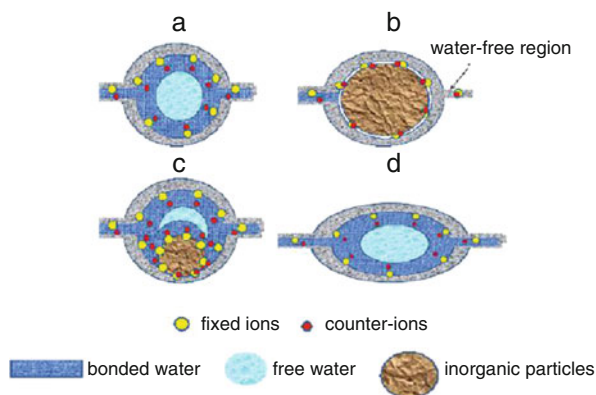

Fig. 16.6 Effect of embedded particles on transport pores: (**a**) pristine polymer, (**b**) complete blockage of the part of clusters and channels (they are free from water), (**c**) partial screening, and (**d**) squeezing affected by swelling pressure from the side of structure defects containing a modifier

Formally, reduction of the L parameter with increase of the modifier content indicates smaller distance between functional groups. However, higher hydration numbers show rebuilding of hydrate shells of fixed and counter-ions due to elongation of transport pores (unwinding of the macromolecule coil). This contradiction is evidently due to blockage of a part of clusters and channels with nanoparticles. As a result, some transport pores are unavailable for water (Fig. 16.6) and excluded from ion exchange. It means that the A_p magnitude is overstated. When the particle is smaller than the transport pores, it partially screens the pore walls. In this case, the counter-ions near the particle surface are involved to ion transport providing the increase of conductivity.

Blockage of the transport pores is confirmed in Ref. [61]. Pore size distributions for clusters have been recalculated as $(1 - m)(dV/d(\log r))$. The recalculated values are higher than the experimental magnitudes for the composites. It means, the modifier decreases water content in transport pores. Structure defects are stretched (see Fig. 16.4a) due to the modifier contribution to swelling pressure.

Comparing with the L parameter, which takes into consideration the value of $A_p^{-0.5}$, the calculation error for hydration number is smaller. It means, the n parameter is more suitable to estimate transformation of porous structure of the polymer constituent. The increase of the n value (see Table 16.1) indicates growth of the distance between functional groups.

Based on obtained results, a shift of the peaks of differential pore size distributions can be explained (see Fig. 16.4b). The pristine polymers contain no charge carriers in voids between gel regions and structure defects. Swelling pressure is provided by fixed and counter-ions only in clusters and channels. As opposed to pristine materials, there are charge carriers in voids between gel regions and structure defects. Electric double layer inside transport pores works as a semipermeable barrier. Thus, additional swelling pressure appears also in the largest pores of polymer. This results in squeezing of transport pores and voids between gel regions, their size becomes smaller (see Fig. 16.6). When non-aggregated nanoparticles are placed in clusters and channels, they provide additional swelling pressure preventing squeezing.

Other parameters, which are obtained from porometric measurements, are as follows: (i) the ratio of volumes of transport and hydrophobic pores (α) [14, 22, 23, 55] and (ii) the ratio of volumes of channels and clusters (γ) [14, 22, 55]. Earlier micropores were excluded from the α parameter; asymmetry of the peaks of differential pore size distributions was also considered [12]. The curves were deconvoluted into Lorentz components in order to estimate transformation of porous structure more exactly.

The change of the α and γ parameters due to embedded particles has been found (see Fig. 16.5b and Table 16.1). This change reflects the ion transport through the composites. Indeed, a growth of the α parameter and reduction of the γ value are characteristic for the composites after the first modification cycle. Simultaneously, electrical conductivity decreases. Further modification causes no sufficient change of these parameters, however, the conductivity grows.

The transformation of the polymer pore structure after the first modification cycles depresses ion transport [12, 22, 23]. This is caused by higher fraction of channels, which contain only bonded water, and by lower fraction of transport pores for the composites comparing with the pristine resin. Improvement of conductivity after the third modification cycle occurs, since the counter-ions of the modifier in clusters and channels are involved into ion transport.

16.7 Evolution of Electrical Conductivity: Functions of Particles

Theoretically, the dependence of the electrical conductivity of composites on the modifier content should obey the percolation theories. Known approaches involve volume fraction and electrical conductivity of modifier and polymer, the shape factor of embedded particles, wettability between the particles and matrix [66]. The theories explain the rapid growth of conductivity after certain critical value of modifier content (so-called percolation threshold). The dependence of conductivity on the modifier fraction can be divided to three regions (Fig. 16.7a). At low modifier content, the conductive particles are separated from each other and the conductivity of the composite is close to that of polymer. The rapid increase of conductivity is related to the formation of the continuous conductive network of modifier. Further increase of its content causes no influence on conductivity.

Let us compare the theory and some experimental results (Fig. 16.7b). Only the composites based on PVDF [67] and poly(2, 6-dimethyl-1, 4-phenyleneoxide) (POO) [71], which contain ZHP derivative [67] and silica [71], are the closest to the percolation model. Regarding the composite containing inert silica, highly conductive PPY is considered as the modifier of inorganic matrix [68]. Here, the falling curves are the inversion of the theoretical dependence (see Fig. 16.7a). The PFM membrane shows the decrease of conductivity with increasing of the ZHP content [63]. The curves for PPY-THP [69] and PFM-CeO$_2$ [70] membranes pass through a maximum. Regarding rigid ion exchange resin, these dependencies show minimum (see Fig. 16.5b). These composites disobey the percolation model due to their heterogeneous structure. Heterogeneity is reinforced with the growth of the modifier content. The conductivity buildup is due to the increase of the
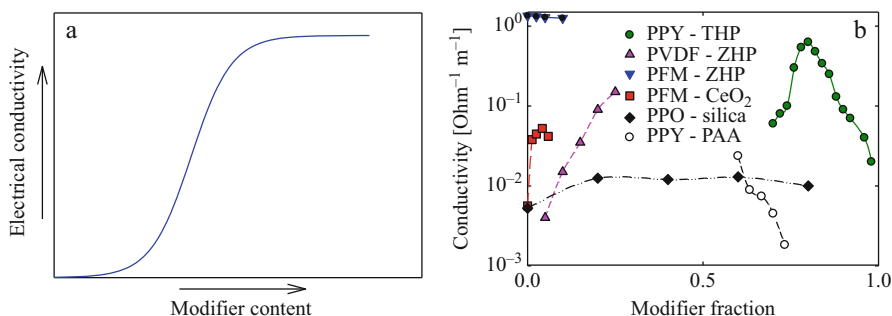

Fig. 16.7 Theoretical (**a**) and experimental (**b**) dependencies of conductivity on the modifier content. The measurements were performed under ambient temperature except the PVDF-ZHP composite (80° C) [67]. Relative humidity was ambient (PPY-PAA [68], PPY-THP [69]), 90% (PVDF-ZHP [67]), and 100% (PFM-ZHP [63]); the materials were immersed with water (PFM-CeO$_2$ [70], PPO-silica [71]) (Here PVDF is polyvinylidene fluoride, POO is poly(2, 6-dimethyl-1, 4-phenyleneoxide), PPY is polypyrrole, and PAA is polyantimonic acid)

amount of non-aggregated silica nanoparticles; the plateau is caused by aggregates [71]. Similarly, embedded ZHP nanoparticles are responsible for the improvement of conductivity [22]. Aggregates and agglomerates depress conductivity after the first modification cycle [22, 23]. Further modification increases conductivity due to elongation of transport pores [23]. These formations make no contributions to transport of counter-ions [22, 23]. However, large particles affect ion transport indirectly changing the porous structure of polymer.

At last, let us consider the functions of embedded particles. Non-aggregated nanoparticles in transport pores improve conductivity, they are also responsible for water retention under elevated temperatures and low humidity (this is important in the case of the membranes applied to fuel cells). According to Yaroslavtsev and Yampolskii, the nanoparticles provide charge selectivity of ion exchange membranes [72]. This is due to screening of the cluster centers (a neutral solution, which contains both counter- and co-ions, is located there [21]). However, small channels protect the cluster-channel system from co-ions. Berezina et al. suggest that voids between gel regions provide transport of co-ions deteriorating charge selectivity of the membranes [20]. High charge selectivity is reached, when the ratio of volumes of transport and non-transport pores is ≈ 0.9 [42]. Aggregates in voids between gel regions depress ion transport. These formations prevent adsorption of organics on hydrophobic fragments of polymer chains. Thus, the aggregates perform protective function as suggested in refs. [13, 14].

Agglomerates increase electroosmotic transport due to appearance of fixed ions in structure defects. They squeeze transport pores providing formation of sorption centers, which are selective toward large ions, such as UO_2^{2+} [55]. The resin containing agglomerates can be used for preferable removal of toxic ions from water containing also Ca^{2+} and Mg^{2+} [23]. Thus, the largest particles are useful rather for ion exchange resins.

16.8   Conclusions

Particles of inorganic ion-exchanger embedded into ion exchange polymer affect its porous structure due to additional swelling pressure. Depending on size and location of the particles, they are able to block, stretch, and squeeze transport pores of the polymer matrix. Thus, the modifier directly or indirectly influences ion transport through the composites. The particle size can be controlled during synthesis. Each type of inorganic particles performs their own function. Non-aggregated nanoparticles in clusters and channels enhance ion transport. They provide also water retention under elevated temperature and low humidity; this expands the temperature diapason of fuel cell operation. Aggregates of nanoparticles in voids between gel regions prevent transport of co-ions and accumulation of organic substances. This improves charge selectivity of ion exchange membranes and enhances their stability against fouling. Agglomerates in structure defects squeeze transport pores; a part of them is excluded from ion transport. Thereby,

formation of the particles of micron size is undesirable for the materials, which are applied to electrochemical processes. However, all types of particles in ion exchange resin enhance their selectivity toward toxic ions.

References

1. Eisenberg A, Yeager HL (eds) (1982) Perfluorinated ionomer membranes. ACS Symp Ser, vol 180. American Chemical Society, Washington
2. Hsu WY, Gierke TD (1983) Ion transport and clustering in nafion perfluorinated membranes. J Membr Sci 13:307–326
3. Kononenko NA, Berezina NP, Vol'fkovich YM et al (1985) Investigation of ion-exchange materials structure by standard porosimetry method. J Appl Chem USSR 58:2029–2033
4. Berezina NP, Kononenko NA, Vol'fkovich YM (1994) Hydrophilic properties of heterogeneous ion-exchange membranes. Russ J Electrochem 30:329–335
5. Guizard C, Bac A, Barboiu M et al (2001) Hybrid organic-inorganic membranes with specific transport properties: Applications in separation and sensors technologies. Separ Purif Technol 25:167–180
6. Kraytsberg A, Eiu-Eli Y (2014) Review of advanced materials for proton exchange membrane fuel cells. Energy Fuels 28:7303–7330
7. Kononenko NA, Fomenko MA, Volfkovich YM (2015) Structure of perfluorinated membranes investigated by method of standard contact porosimetry. Adv Colloid Interf Sci 222:425–435
8. Eisenberg A (1970) Clustering of ions in organic polymers. A theoretical approach. Macromolecules 3:147–154
9. Dreifus B (1986) Clustering and hydration in ionomers. In: Eisenberg A, Bailey FE (eds) Coulombic interaction in macromolecular systems. ACS Symp Ser, vol 302. American Chemical Society, Washington, DC, pp 103–119
10. James PJ, Elliott JA, McMaster TJ et al (2000) Hydration of Nafion studied by AFM and X-ray scattering. J Mater Sci 35:5111–5119
11. Young SK, Trevino SF, Beck Tan NC (2002) Small-angle neutron scattering investigation of structural changes in Nafion membranes induced by swelling with various solvents. J Polym Sci B Polym Phys 40:387–400
12. Dzyazko YS, Ponomareva LN, Volfkovich YM et al (2013) Conducting properties of a gel ionite modified with zirconium hydrophosphate nanoparticles. Russ J Electrochem 49:209–215
13. Dzyazko YS, Rozhdestvenska LM, Vasilyuk SL et al (2017) Composite membranes containing nanoparticles of inorganic ion exchangers for electrodialytic desalination of glycerol. Nanoscale Res Lett 12:438
14. Dzyazko Y, Rozhdestveskaya L, Zmievskii Y et al (2015) Heterogeneous membranes modified with nanoparticles of inorganic ion-exchangers for whey demineralization. Mater Today: Proc 6:3864–3873
15. Kononenko N, Nikonenko V, Grande D et al (2017) Porous structure of ion exchange membranes investigated by various technique. Adv Colloid Interf Sci 246:196–216
16. Helfferich F (1995) Ion exchange. Dover, New York
17. Laporta M, Pegoraro M, Zanderighi L (1999) Perfluorosulfonated membrane (Nafion): FT-IR study of the state of water with increasing humidity. Phys Chem Chem Phys 1:4619–4628
18. Mauritz KA, Moore RB (2004) State of understanding of Nafion. Chem Rev 104:4535–4585
19. Schmidt-Rohr K, Chen Q (2008) Parallel cylindrical water nanochannels in Nafion fuel-cell membranes. Nat Mater 7:75–83
20. Berezina NP, Kononenko NA, Dyomina OA et al (2008) Characterization of ion-exchange membrane materials: properties vs structure. Adv Colloid Interf Sci 139:3–28

21. Nikonenko VV, Yaroslavtsev AB, Pourcelly G (2012) Ion transfer through charged membranes: structure, properties, and theory. In: Ciferri A, Perico A (eds) Ionic interactions in natural and synthetic macromolecules. Wiley, Hoboken, pp 267–335

22. Dzyazko YS, Ponomaryova LN, Volfkovich YM et al (2013) Polymer ion-exchangers modified with zirconium Hydrophosphate for removal of Cd^{2+} ions from diluted solutions. Sep Sci Technol 48:2140–2149

23. Dzyazko YS, Ponomaryova LN, Volfkovich YM et al (2014) Ion-exchange resin modified with aggregated nanoparticles of zirconium hydrophosphate. Morphology and functional properties. Microporous Mesoporous Mater 198:55–62

24. Volfkovich YM (1984) Influence of the electric double layer on the internal interfaces in an ion-exchanger on its electrochemical and sorption properties. Soviet Electrochem 20(5):621–628

25. Mark JE (2007) Physical properties of polymers handbook, 2nd edn. Springer, New York

26. Kimoto K (1983) Water absorption and Donnan equilibria of per-fluoroionomer membranes for the chlor-alkali process. Electrochem Sci Technol 130:334–341

27. Flory PJ, Rehner JJ (1943) Statistical mechanics of cross-linked polymer networks II. Swelling. J Chem Phys 11:521–526

28. Pushpa KK, Nandan D, Iyer RM (1988) Thermodynamics of water sorption by perfluorosulphonate (Nafion-117) and polystyrene–divinylbenzene sulphonate (Dowex 50W) ion-exchange resins at 298 ± 1 K. J Chem Soc Faraday Trans 1(84):2047–2056

29. Tripathi BP, Shahi VK (2011) Organic–inorganic nanocomposite polymer electrolyte membranes for fuel cell applications. Prog Polym Sci 36:945–979

30. Sanchez C, Julián B, Belleville P et al (2005) Applications of hybrid organic-inorganic nanocomposites. J Mater Chem 15:3559–3592

31. Perlova N, Dzyazko Y, Perlova O et al (2014) Formation of zirconium hydrophosphate nanoparticles and their effect on sorption of uranyl cations. Nanoscale Res Lett 12:209. https://doi.org/10.1186/s11671-017-1987-y

32. Perlova O, Dzyazko Y, Halutska I et al (2018) Anion exchange resin modified with nanoparticles of hydrated zirconium dioxide for sorption of soluble U(VI) compounds. Springer Proc Phys 210:3–15

33. Myerson AS (ed) (2002) Handbook of industrial crystallization. Butterworth-Heinemann, Woburn

34. Ekberg C, Källvenius G, Albinsson Y et al (2004) Studies on the hydrolytic behavior of zirconium(IV). J Solut Chem 33(1):47–79

35. Kobayashi T, Sasaki T, Takagi I et al (2007) Solubility of zirconium(IV) hydrous oxides. J Nucl Sci Technol 44(1):90–94

36. Dzyazko YS, Volfkovich YM, Sosenkin VE et al (2014) Composite inorganic membranes containing nanoparticles of hydrated zirconium dioxide for electrodialytic separation. Nanoscale Res Lett 9:271. https://doi.org/10.1186/1556-276X-9-271

37. Myronchuk VG, Dzyazko YS, Zmievskii YG et al (2016) Organic-inorganic membranes for filtration of corn distillery. Acta Periodica Technologica 47:153–165

38. Zmievskii Y, Rozhdestvenska L, Dzyazko Y et al (2017) Organic-inorganic materials for baromembrane separation. Springer Proc Phys 195:675–686

39. Zhang Q, Jiang P, Pan B et al (2009) Impregnating zirconium phosphate onto porous polymers for lead removal from waters: effect of nanosized particles and polymer chemistry. Ind Eng Chem Res 48:4495–4499

40. Jia K, Pan B, Lv L et al (2009) Impregnating titanium phosphate nanoparticles onto a porous cation exchanger for enhanced lead removal from waters. J Colloid Interface Sci 331:453–457

41. Pan B, Pan B, Chen X et al (2006) Preparation and preliminary assessment of polymer-supported zirconium phosphate for selective lead removal from contaminated water. Water Res 40(15):2938–2946

42. Yang C, Srinivasan S, Aricò AS et al (2001) Composite Nafion/zirconium phosphate membranes for direct methanol fuel cell operation at high temperature. Electrochem Solid-State Lett 4:A31–A34

43. Chabé J, Bardet M, Gébel G (2012) NMR and X-ray diffraction study of the phases of zirconium phosphate incorporated in a composite membrane Nafion®-ZrP. Solid State Ionics 229:20–25
44. Nicotera I, Khalfan A, Goenaga G et al (2008) NMR investigation of water and methanol mobility in nanocomposite fuel cell membranes. Ionics 14:243–253
45. Dzyazko YS, Trachevskii VV, Rozhdestvenskaya LM et al (2013) Interaction of sorbed Ni(II) ions with amorphous zirconium hydrogen phosphate. Russ J Phys Chem A 87(5):840–845
46. Nussinovitch A (2010) Polymer macro- and micro-gel beads: fundamentals and applications. Springer, New York/Dordrecht/Heidelberg/London
47. Gregg SJ, Sing KSW (1991) Adsorption, surface area and porosity. Academic Press, London
48. Harland CE (1994) Ion exchange-theory and practice, 2nd edn. RSC Publisher, Letchworth
49. Brun M, Quinson JF, Blanc R et al (1981) Caractérisation texturale de résines en milieu réactionnel. Macromol Chem Phys 182:873–882
50. Rouquerol J, Baron G, Denoyel R et al (2011) Liquid intrusion and alternative methods for the characterization of macroporous materials (IUPAC technical report). Pure Appl Chem 84:107–136
51. Volfkovich YM, Bagotsky VS (2014) Experimental methods for investigations of porous materials and powders. In: YuM V, Filippov AN, Bagotsky VS (eds) Structural properties of different materials and powders used in different fields of science and technology. Springer, London/Heidelberg/New York/Dordrecht, pp 1–8
52. Volfkovich YM, Sosenkin VE (2012) Porous structure and wetting of fuel cell components as the factors determining their electrochemical characteristics. Russ Chem Rev 81:936–959
53. Volfkovich YM, Sakars AV, Volinsky AA (2005) Application of the standard porosimetry method for nanomaterials. Int J Nanotechnol 2:292–302
54. Dzyazko YS, Volfkovich YM, Ponomaryova LN et al (2016) Composite ion-exchangers based on flexible resin containing zirconium hydrophosphate for electromembrane separation. J Nanosci Technol 2:43–49
55. Dzyazko YS, Perlova OV, Perlova NA et al (2017) Composite cation-exchange resins containing zirconium hydrophosphate for purification of water from U(VI) cations. Desalin Water Treat 69:142–152
56. Dzyazko YS, Ponomareva LN, Volfkovich YM et al (2012) Effect of the porous structure of polymer on the kinetics of Ni^{2+} exchange on hybrid inorganic-organic ionites. Russ J Phys Chem 86:913–919
57. Zabolotskii VI, Protasov KV, Sharafan MV (2010) Sodium chloride concentration by electrodialysis with hybrid organic-inorganic ion-exchange membranes: an investigation of the process. Russ J Electrochem 46:979–986
58. Novikova SA, Safronova EY, Lysova AA et al (2010) Influence of incorporated nanoparticles on the ionic conductivity of MF-4SC membrane. Mendeleev Commun 20:156–157
59. Nagarale RK, Gohil GS, Shahi VK et al (2004) Organic-inorganic hybrid membrane: thermally stable cation-exchange membrane prepared by the sol-gel method. Macromolecules 37:10023–10030
60. Khan AA, Khan A, Inamuddin (2007) Preparation and characterization of a new organic–inorganic nano-composite poly-o-toluidine Th(IV) phosphate: its analytical applications as cation-exchanger and in making ion-selective electrode. Talanta 72(2):699–710
61. Dzyazko Y, Ponomarova L, Volfkovich Y et al (2016) Influence of zirconium hydrophosphate nanoparticles on porous structure and sorption capacity of the composites based on ion exchange resin. Ch Ch Technol 19:329–335
62. Ponomarova L, Dzyazko Y, Volfkovich Y et al (2018) Effect of incorporated inorganic nanoparticles on porous structure and functional properties of strongly and weakly acidic ion exchangers. Springer Proc Phys 214:63–77
63. Sahu AK, Bhat SD, Pitchumani S et al (2009) Novel organic–inorganic composite polymer-electrolyte membranes for DMFCs. J Membr Sci 345:305–314

64. Alberti G, Casciola M, Capitani D et al (2007) Novel Nafion–zirconium phosphate nanocomposite membranes with enhanced stability of proton conductivity at medium temperature and high relative humidity. Electrochim Acta 52:8125–8132
65. Bryk MT, Zabolotsky VI, Atamanenko D et al (1989) Structural inhomogeneity of ion-exchange membranes in swelling state and methods of its investigations. Khim Tekhnol Vody 11:491–498
66. Taherian R (2016) Experimental and analytical model for the electrical conductivity of polymer-based nanocomposites. Compos Sci Technol 123:17–31
67. Casciola M, Alberti G, Ciarletta A et al (2005) Nanocomposite membranes made of zirconium phosphate sulfophenylenphosphonate dispersed in polyvinylidene fluoride: preparation and proton conductivity. Solid State Ionics 176:2985–2989
68. Khan AA, Alam MM, Inamuddin et al (2004) Electrical conductivity and ion-exchange kinetic studies of a crystalline type 'organic–inorganic' cation-exchange material: polypyrrole/polyantimonic acid composite system, (Sb_2O_5) $(-C_4H_2NH-)\cdot nH_2O$. J Electroanal Chem 572:67–67
69. Khan AA, Paquiza L (2011) Electrical behavior of conducting polymer based 'polymeric–inorganic' nanocomposite: polyaniline and polypyrrole zirconium titanium phosphate. Synth Met 161:899–905
70. Kuznetsova EV, Safronova EY, Ivanov VK et al (2013) Transport properties of hybrid materials based on MF-4SC perfluorinated ion exchange membranes and nanosized ceria. Nanotechnol Russ 8:461–465
71. Tong X, Zhang B, Fan Y et al (2017) Mechanism exploration of ion transport in nanocomposite cation exchange membranes. ACS Publ. Appl Mater Interfaces 9:13491–13499
72. Yaroslavtsev AB, Yampolskii YP (2014) Hybrid membranes containing inorganic nanoparticles. Mendeleev Commun 24:319–326